



Published in final edited form as:

*J Electrochem Soc.* 2008 ; 155(5): K91–K95. doi:10.1149/1.2868772.

## Electrochemical Properties of Carbon Nanoparticles Entrapped in Silica Matrix

Sangho Bok, Arnold A. Lubguban, Yuanfang Gao, Shantanu Bhattacharya, Venu Korampally, Maruf Hossain, Kevin D. Gillis<sup>†</sup>, and Shubhra Gangopadhyay<sup>\*</sup>

Department of Electrical and Computer Engineering, University of Missouri-Columbia 349 Engineering Building West, Columbia Missouri 65211-2300 USA

<sup>†</sup>Department of Biological Engineering, Dalton Cardiovascular Research Center, University of Missouri - Columbia

### Abstract

Carbon-based electrode materials have been widely used for many years for electrochemical charge storage, energy generation, and catalysis. We have developed an electrode material with high specific capacitance by entrapping graphite nanoparticles into a sol-gel network. Films from the resulting colloidal suspensions were highly porous due to the removal of the entrapped organic solvents from sol-gel matrix giving rise to high Brunauer-Emmett-Teller (BET) specific surface areas (654 m<sup>2</sup>/g) and a high capacitance density (~37 F/g). An exponential increase of capacitance was observed with decreasing scan rates in cyclic voltammetry studies on these films suggesting the presence of pores ranging from micro (< 2 nm) to mesopores. BET surface analysis and scanning electron microscope images of these films also confirmed the presence of the micropores as well as mesopores. A steep drop in the double layer capacitance with polar electrolytes was observed when the films were rendered hydrophilic upon exposure to a mild oxygen plasma. We propose a model whereby the microporous hydrophobic sol-gel matrix perturbs the hydration of ions which moves ions closer to the graphite nanoparticles and consequently increase the capacitance of the film.

### Introduction

Carbon-based electrode materials are widely used in research and industry for a variety of applications. For example high porosity carbon matrices have been heavily explored in building ultra-capacitors particularly due to their high-energy storage density and low cost.[1] The energy storage density is prominent in these materials due to a large available surface area of the porous matrix. Some other applications include air and water purification, gas separation, catalysis, and chromatography. Most of these applications utilize exceptional properties of porous carbon materials such as high surface area, large pore volumes, chemical inertness and good mechanical stability.[2] In addition, carbon-based electrodes have desirable properties for electrochemistry such as a large potential window between the water splitting reactions, low or constant background current and fast electron-transfer kinetics.[3]

There are several routes to synthesis of porous carbon such as pyrolysis or carbonization (under N<sub>2</sub> environment) of an organic precursor to obtain carbon inside the mesopores of silica templates.[4] Alternatively, the sol-gel method has been used to assemble porous carbon flakes through a hydrolysis and condensation process using a silica source such as TEOS (tetraethoxysilane, Si(OEt)<sub>4</sub>).[5] The sol-gel approach has been widely used as a versatile

\*Corresponding author. Email: GangopadhyayS@missouri.edu Tel: (573) 882-4070

method to produce inorganic-organic electrodes and electrochemical sensors for decades.[3] Porous organosilicate matrices are an excellent inert support medium because of their lack of electroactivity. Therefore much research effort has focused on immobilizing surface functional groups, chemical modifiers or redox species within the matrices to enhance the electroactivity of the immobilized species. Electroactive silicate composites can be obtained by incorporating inorganic, organic, or biological moieties into sol-gel precursors and allowing this to gelate following film deposition.[3] For example, Oskam, et al. have used micron-sized graphite particles to obtain 0.1 cm thick films with  $1 \text{ S cm}^{-1}$  conductivity with pure capacitive behavior on fluorine-doped tin oxide, copper, and steel substrates.[6] Berguiga, et al. have incorporated functionalized multi-walled carbon nanotubes (CNT) in a sol-gel process.[7]

We have successfully entrapped nano-sized (average diameter 55 nm with maximum diameter less than 100 nm) graphite particles in a sol-gel matrix and have obtained relatively large values of double layer capacitance due to the combination of hydrophobicity of sol-gel and non-hydrophobicity of graphite nanoparticles as well as the enhanced surface area of the films. We also observed that the capacitance increased exponentially when the micropores in porous silica dominated the redox reaction in the double layer capacitor. We have further been able to substantially reduce the capacitance of the films by exposure to a low-power oxygen plasma. These properties could be used for many applications including sensitive electrochemical detection of analytes and fabrication of supercapacitors.

## Materials and Methods

### Thin Film Electrode Preparation

The sol-gel precursor preparation and hydrolysis were performed sequentially in a controlled-temperature environment. For the sol-gel process, precursor solutions were prepared under acidic conditions in two steps.[8] The method was described earlier by de Theije *et al* [8] where the precursor solution was diluted with ethanol to prolong the gelling time so that a thin film of this solution could be spun on a substrate. In step one a typical starting mixture containing TEOS (tetraethoxysilane,  $\text{Si}(\text{OEt})_4$ ), MTMS (methyltrimethoxysilane,  $\text{Si}(\text{OMe})_3\text{CH}_3$ ), water, HCl, and anhydrous ethanol (99%) was heated at  $60^\circ\text{C}$  for 90 min. The amount of MTMS and TEOS were mixed in a 50 mol % basis. A total of 0.25 mol of water were added per alkoxy group, and ethanol and HCl were added in molar ratios of 3 and  $5 \times 10^{-5}$  relative to the silicate precursors thus hydrolyzing the silicates partially, while preventing significant condensation. This mixture was then diluted with ethanol, water and HCl. The prepared precursor solution was allowed to age for about three days for further polycondensation. This step essentially enhanced the silica matrix formulation (Fig. 1). After polycondensation, 0.3 grams of graphite nanoparticles in powder form 55 nm mean diameter (M/s Nanostructured and Amorphous Materials, Inc.) sonicated in 5 ml Ethanol for 4 hours were added to the 5 ml of polycondensed sol-gel and was allowed to gently mix for a short time to form a colloidal suspension. Several pre-cleaned glass substrates were drop casted with the sol-gel graphite mixture and the films were heated to  $60^\circ\text{C}$  for 15 minutes for solvent removal and hardening. The graphite/sol-gel thin films were heated under a nitrogen environment to  $400^\circ\text{C}$  for about an hour. The electrochemical analyses were performed on an electrochemical analyzer with all electrolytes mixed with high purity water.

### Oxygen Plasma Treatment

As-prepared graphite thin film electrodes were treated with  $\text{O}_2$  plasma for various exposure times. The plasma equipment was performed in M/s Harrick Plasma (Model PDC-32G). Low RF power of 6.8W was used for  $\text{O}_2$  plasma treatment. Thin films with different exposure times were evaluated for their electrochemical behavior.

## Contact Angle Measurement

We have correlated the change of contact angle using the sessile drop measurement method on the plasma-exposed film surface with the corresponding change in its capacitance value. For the oxygen plasma treated samples, contact angle measurements were performed within one minute of treatment. The contact angle was calculated from the image of the droplet.

## Fourier Transform Infrared (FTIR) Spectroscopic Measurements

A Nicolet-4700 FTIR spectrometer was utilized for spectral measurements of the as-prepared and plasma exposed films on low resistivity silicon substrates in the transmission mode.

## Tests and Characterization

The resistivity of the films was obtained from a four-point measurement. The film thickness was determined using a profilometer and was later confirmed by scanning electron microscope (SEM). Cyclic voltammetry was performed on the films using a CHI Model 800B Electrochemical Analyzer. The thin films, a platinum wire and a Ag-AgCl segment (0.8 mm dia.  $\times$  8 mm) were used as working, counter and reference electrodes, respectively. Cyclic voltammograms were obtained with all the three electrodes immersed within a conventional electrochemical cell made by pasting a plastic annular ring with an inner diameter of 8 mm (Fig. 2). All chemicals employed were analytical reagent grade and the measurements were taken at room temperature 22-23°C.

## Results and Discussion

### Thin Film Electrode Properties

The importance of using sol-gel precursor in the synthesis of carbon-based electrode materials lies in the fact that the composite material can benefit from the excellent properties of the silicate backbone. As pointed out earlier, the backbone is itself electrochemically inactive but provides an environment for electron percolation through the interconnected grains of carbon. [3] The graphite/sol-gel electrodes showed a resistivity of 0.0516  $\Omega$ -cm, suggestive of the conductive nature of the carbon nanostructures. Some investigators reported that long range hydrophobic forces in aqueous solutions can be obtained at surface contact angle,  $\theta \geq 90^\circ$ . [9-11] The as-prepared graphite/sol-gel thin film electrodes were superhydrophobic with contact angles of 126.8°. This can be attributed to the addition of hydrophobic organofunctional monomers such as methyltrimethoxysilane (MTMS), which form hydrophobic organosilicates as well as the micron-scale roughness arising from the highly porous matrix structure. The surface area of the graphite/sol-gel samples measured by the BET method was  $\sim 654$  m<sup>2</sup>/g whereas the surface area of the graphite nanoparticles was  $\sim 60$  m<sup>2</sup>/g. The thin film contains 40% of porous silica binding 60% of graphite nanoparticles. Figure 3 shows the pore size distribution for the graphite nanoparticle/sol-gel composite film. The distribution is bimodal in nature with 17 % micropores less than 2 nm in diameter. The SEM image in figure 4(a) presents the highly porous structure of the sample. Figure 4(b) shows mesopores in the samples having diameters less than 5 nm. The graphite nanoparticles used are spherical and have an average diameter of 55 nm as shown in the TEM image (Fig. 4(c)).

### Capacitance Analysis

The double-layer capacitance,  $C$  was measured from the current response to a triangular voltage waveform. The electrode area over which the measurements were performed was 0.501 cm<sup>2</sup> and the total mass of the graphite nanoparticles enclosed within this area was 0.072 mg. Different scan rates (1, 2, 5, 10, 20, 50, 100, and 200 mV/s) for the triangular waveform were applied and the change in current ( $\Delta i$ ) was measured from the plateau region of the cyclic voltammogram (Fig. 5). The specific capacitance (F/gram) was calculated from the relationship

$$C = \frac{\Delta i}{2wm} \quad (1)$$

where  $w$  is the scan rate and  $m$  is the mass of graphite nanoparticles in the sample. The specific capacitance per unit mass for our films with a BET surface area of  $654 \text{ m}^2/\text{g}$  was calculated to be  $36.7 \text{ F/g}$  at a scan rate of  $1 \text{ mV/s}$ . In contrast, Oskam et al. report a specific capacitance of  $0.24 \text{ F/g}$  for films consisting of micron-sized carbon particles embedded in a silica matrix. The BET surface area of their films was  $3.5 \text{ m}^2/\text{g}$ . [6] The two orders of magnitude increase in the specific capacitance of our films can be attributed to the increased specific surface area because of the use of graphite nanoparticles and the micro as well as mesopores of our sol-gel network. In addition, we have observed that the hydrophobic nature of the sol-gel matrix plays a significant role in the high value of specific capacitance with aqueous solutions. We hypothesize that this large value of capacitance for the graphite nanoparticle/sol-gel composite results from having non-hydrophobic graphite nanoparticles embedded within a hydrophobic porous matrix (Fig. 6(a)). This restricts the solvated ions to tightly confined spaces close to the surface of the graphite electrode resulting in small separations between the electrolytes and the graphite particle surface and a significant increase in the double layer capacitance (Fig. 6(b)). A similar super capacitance effect was observed by Chmiola, et al. [12] when the pore size of the carbon electrodes was made so small as to approach the diameter of the solvated ions. The resulting ‘squeezing’ of the solvated ions within the pores brings them closer to the electrode surface thereby increasing the capacitance.

In our case, due to the tight confinement of the electrode particles within the silica matrix as illustrated in figure 6(a), the solvated ions are further confined around the hydrophilic graphite electrode surface, as shown in figure 6(b), similar to the effect observed by Chmiola, et al. [12] The importance of the hydrophobic matrix in determining the high specific capacitance in aqueous solutions is supported by experiments we performed demonstrating a much smaller capacitance when using  $\text{O}_2$  plasma-exposed films with aqueous electrolyte solutions. The specific capacitances per unit mass of as-prepared films with different thicknesses were found to be same (data not shown) confirming the whole films were involved in the process.

### Effect of Oxygen Plasma Exposure on the Sol-Gel Graphite Films

Low power oxygen plasma treatment of these films has been performed to render them hydrophilic by the removal of  $-\text{CH}_3$  groups from the sol-gel matrix. The films were exposed for different times and the specific capacitance per unit mass was measured immediately after each exposure. Figure 7 gives the capacitance versus oxygen plasma treatment time plots which shows a dramatic drop in the capacitance from a relatively high value of  $24.4 \text{ F/g}$  for the as-prepared films to as low as  $0.54 \text{ F/g}$  at  $20 \text{ mV/s}$  after a 5 second exposure to  $\text{O}_2$  plasma. This behavior is consistent with our proposed model where the hydrophobicity of the porous matrix is critical for the high specific capacitance of the material. FTIR spectra and contact angle of the films were obtained at different times of exposure to oxygen plasma to probe the mechanism for the change in specific capacitance. In figure 8, we compared the cyclic voltammograms of as-prepared and oxygen plasma treated films in  $1\text{M KCl}$ . The solid line and dotted line indicate the as-prepared film and oxygen plasma treated films, respectively. After an initial sudden drop of capacitance during the first few seconds of plasma exposure, the capacitance per unit mass begins to increase with continuing exposure, although never reaching the values obtained with the as-prepared films (Fig 7). This can be attributed to change in surface texture with increased exposure times (Fig. 9(b)). The maximum capacitance observed in 95 seconds of exposure was calculated to be  $5.88 \text{ F/g}$ . Figure 9 shows SEM micrographs of before and after oxygen plasma exposed films. Visible damage to the film surface was observed with 30 minutes of plasma exposure (Fig. 9(b)). SEM analysis of the films’ cross-section suggested a

substantial decrease in the film thickness from an initial value of 1.65 microns to 1.35 microns after the 30 minute exposure (Fig. 9(d)).

### Contact Angle Studies of the Films

We have characterized the hydrophobicity of surfaces exposed to oxygen with contact angle measurements. The as-prepared surface of the sol-gel entrapped graphite film is highly hydrophobic (contact angle = 126.8 °). The contact angle of the film after 5 seconds of exposure to oxygen plasma drops to approximately 5.29 °. This value does not change significantly with further increases in plasma exposure time (Fig. 10).

### FTIR Spectroscopy of the Film Surfaces

We have investigated the effect of oxygen plasma by performing an FTIR characterization of the films. Figure 11 (a) shows FTIR spectra of the as-prepared films and O<sub>2</sub> plasma exposed films. The peak at 1574 cm<sup>-1</sup> corresponds to the graphitic C=C stretching band while the peak at 1050 cm<sup>-1</sup> is attributed to Si-O stretching.[13] Figure 11(b) presents the FTIR spectra at the region 1280-1250 cm<sup>-1</sup> that is attributed to the presence of Si(CH<sub>3</sub>)<sub>n</sub> (where n=1, 2, 3, or 4) in the MTMS precursor. The area under the curve was computed before and after exposing the films to oxygen plasma for 30 minutes and we observed a 42.1% decrease in the area of the Si(CH<sub>3</sub>)<sub>n</sub> peak following oxygen plasma exposure. The contact angle and FTIR measurements confirm that the film changes from superhydrophobic to hydrophilic due to the removal of CH<sub>3</sub> groups by oxygen plasma.

### Dependence of specific capacitance on the scan rate

We have observed an exponential relation between scan rates and specific capacitance which is consistent with the porous nature of our sol-gel network consisting of meso as well as micropores (Fig. 12). Yang et al. reported that in the case of porous carbon electrodes, mesoporous capacitance was mainly measured in fast scan rate whereas sum of micro and mesoporous capacitances was measured in slow scan rate.[14] At slow scan rates ions have time to move in and out of micropores whereas this mass transfer process is too slow to respond to fast scan rates. Also, since the micropores are smaller in size than the solvated ions, ions entering micropores in response to an electric field become partially dehydrated and are thus closer to the electrode surface than what occurs in bulk solution. This close apposition between the ion and the electrode leads to an increase in specific capacitance similar to that previously described in porous carbon electrodes.[12]. The dependence of capacitance on scan rate was observed in as-prepared films and O<sub>2</sub> plasma treated films (Fig. 12) whereas the capacitance of nonporous films such as platinum did not show scan-rate dependence (data not shown).

### Summary and Conclusion

In this communication we have demonstrated that entrapment of carbon nanoparticles in sol-gel binders can be utilized as charge storage devices with desirable properties of high conductivity, high specific capacitance and good physical stability. We have achieved high capacitance values by entrapping graphite nanoparticles in hydrophobic porous organosilicate matrix. The restriction of the solvated ions to tightly confined spaces close to the graphite electrode surface resulted in the high capacitance values. Furthermore, O<sub>2</sub> plasma treatment of the as-prepared films rendered the surfaces hydrophilic and resulted in a corresponding dramatic drop in capacitance values. We also observed that the specific capacitance depended on scan rate, which can be attributed to the presence of micropores in the silica matrix.

### Acknowledgements

This work was supported by the National Institutes of Health grant NS048826.

## References

1. Dietz, SD.; Nguyen, V. Proceedings of the 2002 NSF Design, Service and Manufacturing Grantees and Research Conference; Tampa, FL. 2002;
2. Ryoo R, et al. *Advanced Materials* 2001;13(No 9):677–681.
3. Rabinovich L, Lev O. *Electroanalysis* 2001;13(No 4):265–275.
4. Lee J, et al. *Carbon* 2005;43:2536–2543.
5. Liu Y, et al. *Thin Solid Films* 1999;353:124–128.
6. Oskam G, Searson PC. *J. Phys. Chem. B* 1998;102:2464–2468.
7. Berguiga L, et al. *Optical Materials* 2006;28:167–171.
8. de Theije FK, et al. *J. Phys. Chem. B* 2003;107:4280–4289.
9. Christenson HK, et al. *J. Phys. Chem* 1990;94:8004–8006.
10. Kurihara K, Kunitake T. *J. Am. Chem. Soc* 1992;114:10927–10933.
11. Christenson HK, Claesson PM. *Advances in Colloid and Interface Science* 2001;91:391–436.
12. Chmiola J, et al. *Science* 2006;313:1760–1763. [PubMed: 16917025]
13. Socrates, G. J. Wiley & Sons Ltd.; 1994.
14. Yang K, Yiacoumi S, Tsouris C. *J. Electroanal. Chem* 2003;540:159–167.

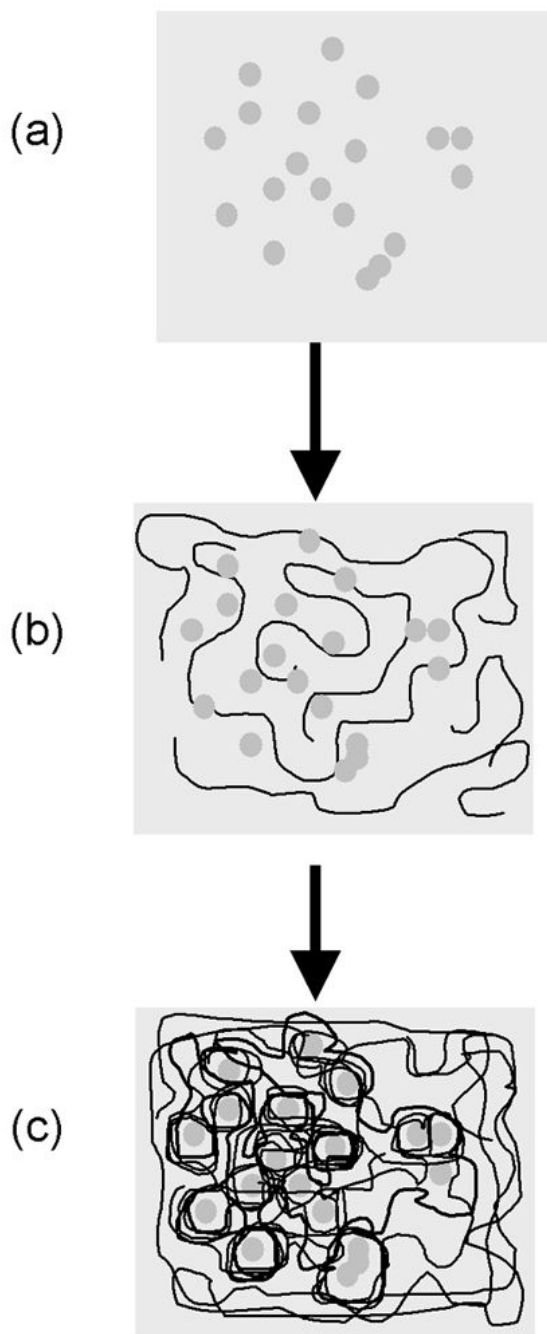


**Fig. 1.** Mechanism of incorporation and entrapment of carbon nanostructures in silica matrix. (a) Incorporation of carbon nanostructures into the sol-gel precursor by gentle mixing, (b) Formation of siloxane bonds around the nanostructures, and (c) Further polycondensation and silica matrix making a stable network of support around the nanostructures.

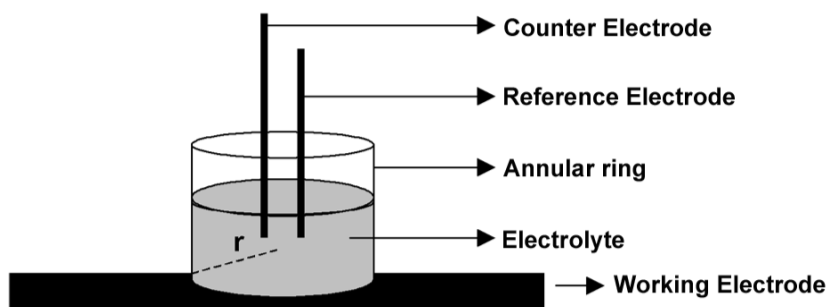


**Fig. 2.** Set-up for the electrochemical analysis of sol-gel carbon nanostructure-based thin film electrodes. Annular ring was employed to hold electrolytes. Counter and reference electrodes were immersed in electrolytes and the as prepared sample was utilized as a working electrode.

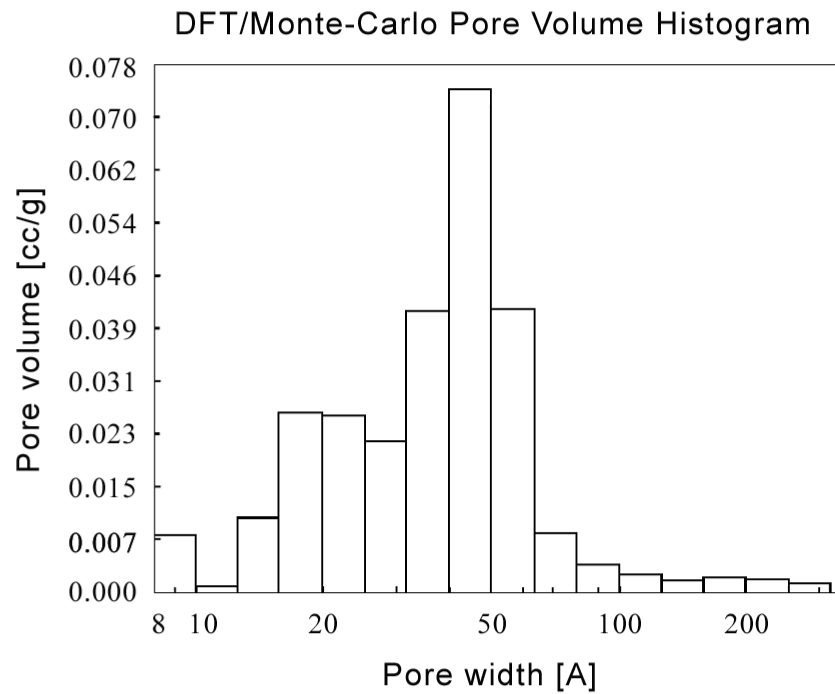


**Fig. 3.** Pore volume histogram shows that the size of the pores of as-prepared films is 5 nm in width. Based on the histogram, these films contain 17 % of pores in less than 2 nm in diameter. The pore size distribution shows bimodal at 2 nm and 5 nm.

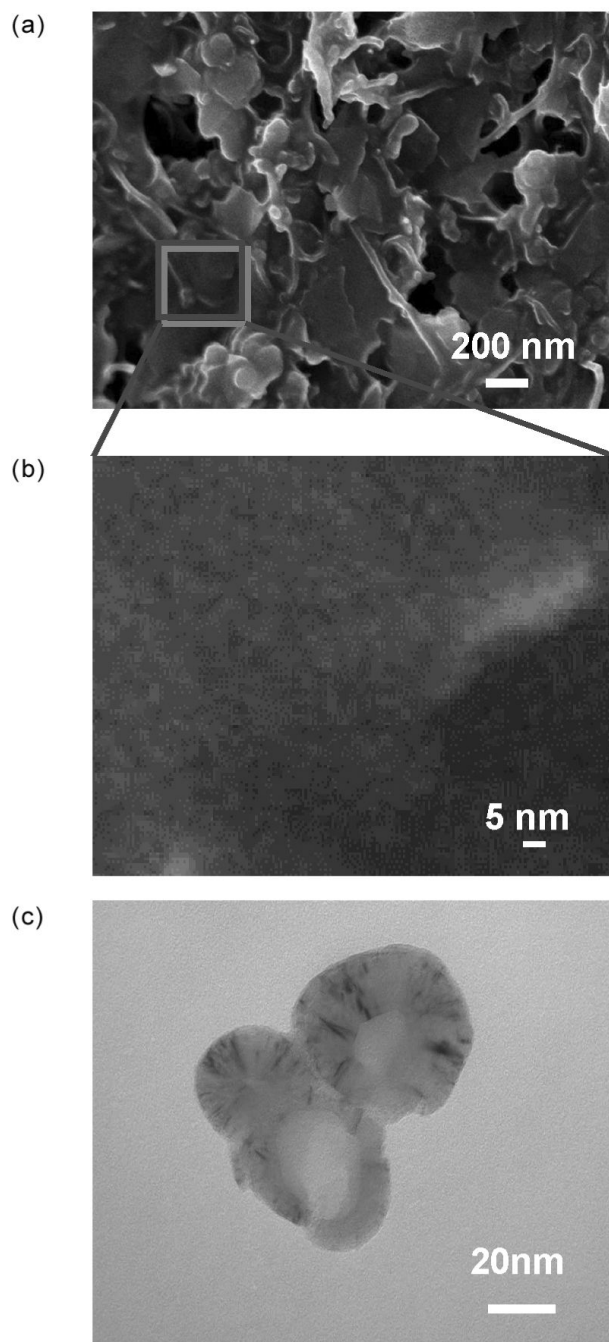


**Fig. 4.** (a) SEM image of sol-gel graphite thin film electrode showing a highly porous surface, (b) expanded SEM image of sol-gel graphite thin film showing mesopores with diameter less than 5nm and (c) TEM image of spherical graphite nanoparticles of 55 nm average diameters is shown.

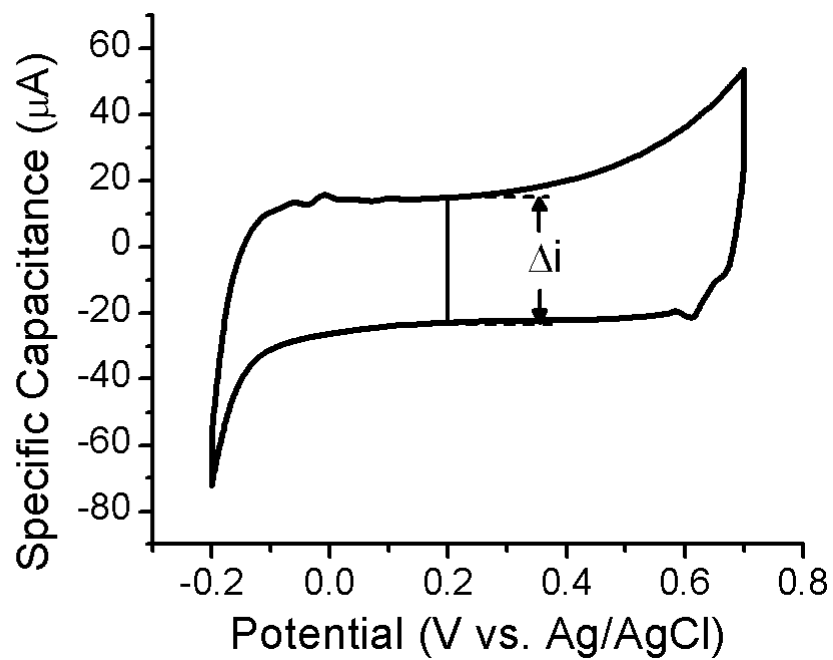


**Fig. 5.** Cyclic voltammogram for as-prepared film electrode in 1M KCl at a scan rate,  $\nu$  of  $10\text{mV s}^{-1}$  is shown.  $\Delta i$  is taken at a point in flat region.

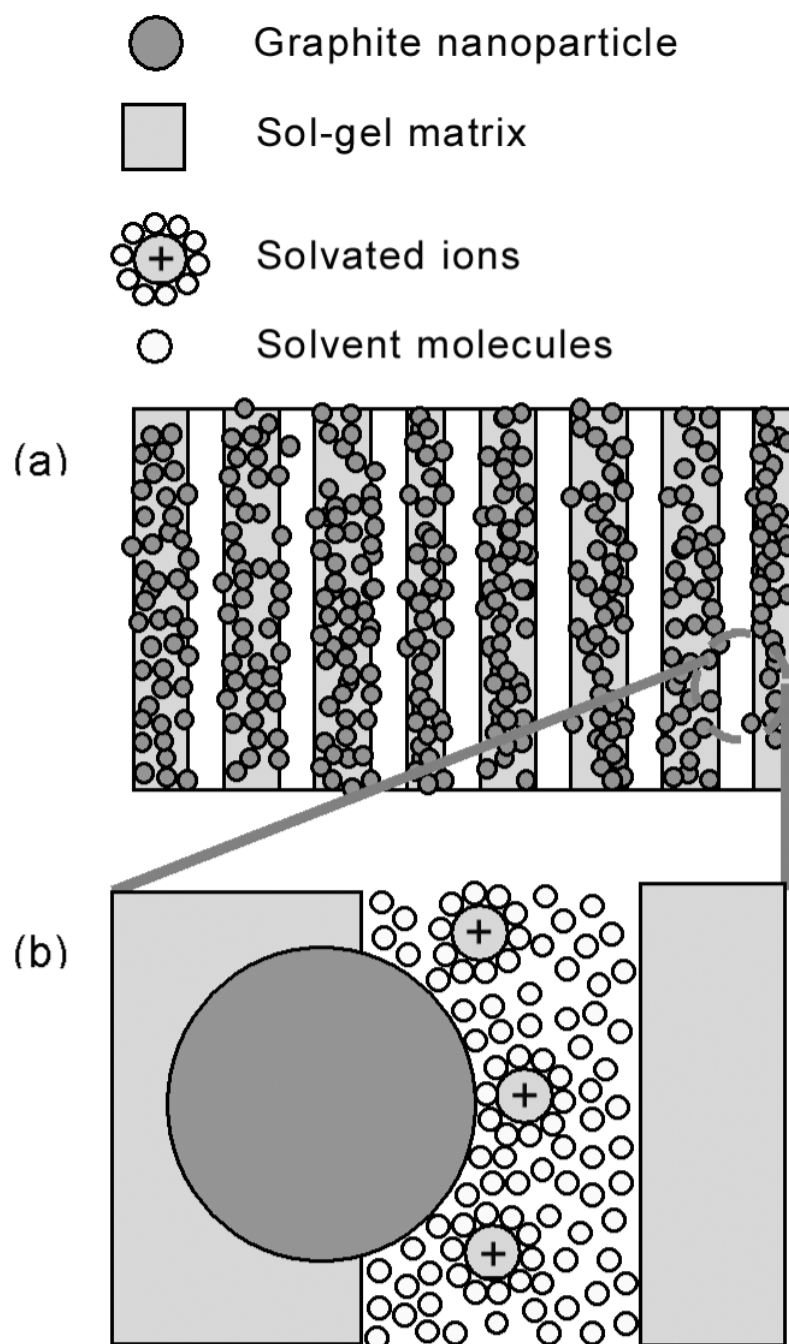


**Fig. 6.** (a) schematic drawing of the as-prepared films show that meso and micropores contain many graphite nanoparticles embedded and (b) a zoomed region of the circle in (a) shows decrease of the distance between the solvated ion center and the surface of graphite nanoparticle due to hydrophobicity.

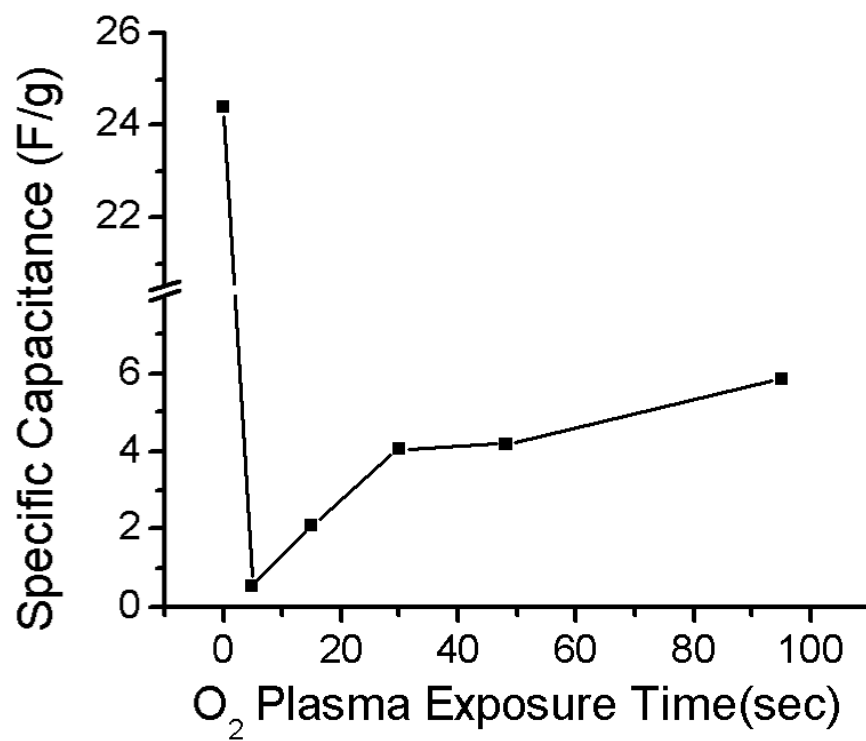


**Fig. 7.** Trend of the change in specific capacitance per unit mass of the as-prepared film and the same film exposed to different times with low RF O<sub>2</sub> plasma shows sudden decrease in specific capacitance after 5 second exposure. The specific capacitance starts to increase with continuing exposure due to change in surface texture.

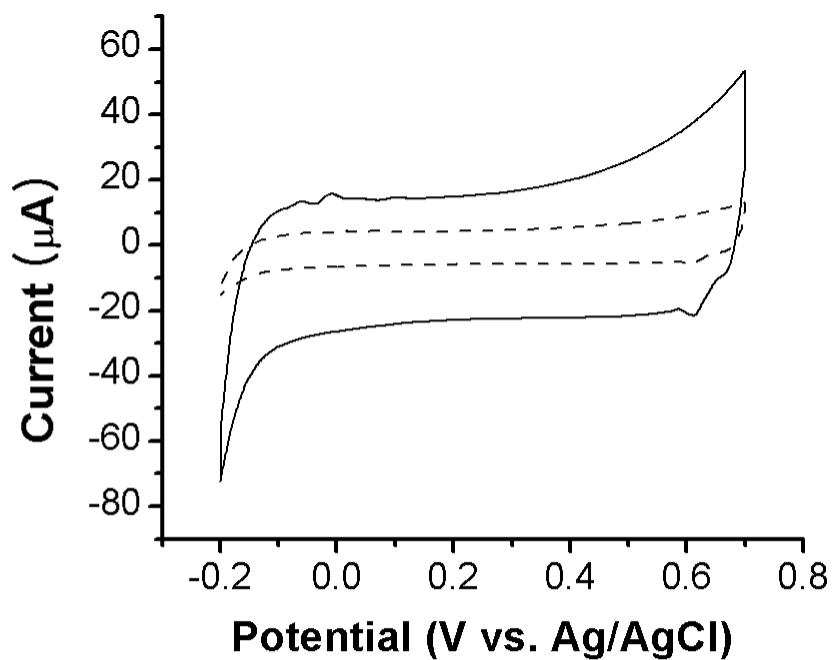


**Fig. 8.** CV curves of sol-gel graphite thin film electrode on glass substrates at scan rate of 10mV/s. The solid line and dotted line show the cyclic voltammetry curves of as-prepared films and O<sub>2</sub> plasma treated films with 1 M KCl, respectively.

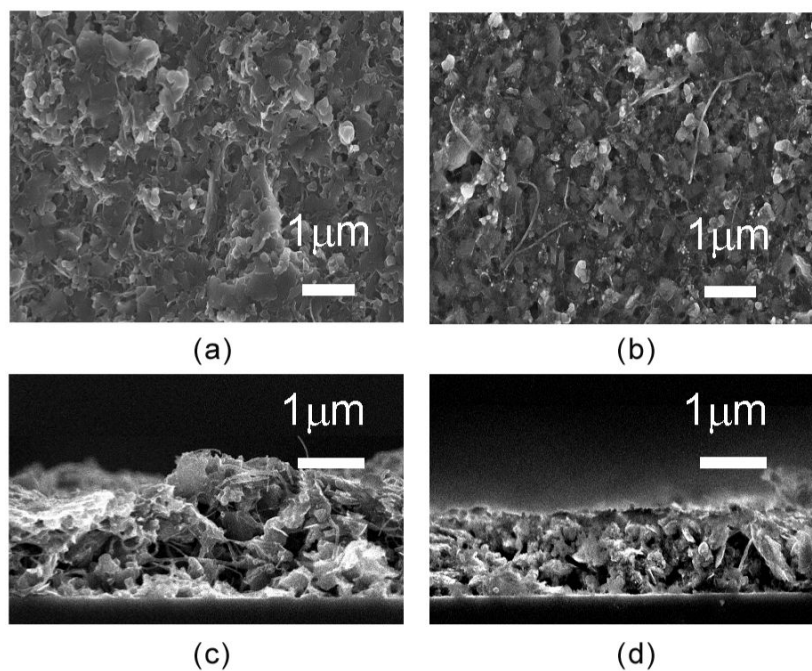


**Fig. 9.** SEM micrographs of sol-gel graphite thin film electrode: top view(a), cross section(c) prior to and top view(b), cross section(c) after 30 minutes exposure to O<sub>2</sub> plasma. The average thickness before oxygen plasma treatment was 1.68  $\mu\text{m}$  and the treatment reduced the thickness to 1.34 $\mu\text{m}$ . Surface roughness increases with exposure with graphite nanoparticles come out of the surface more prominently.

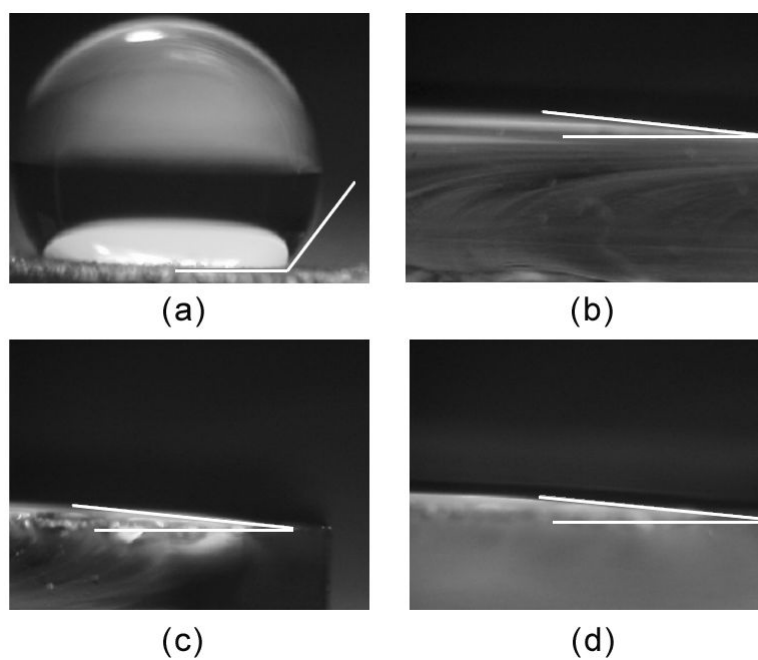
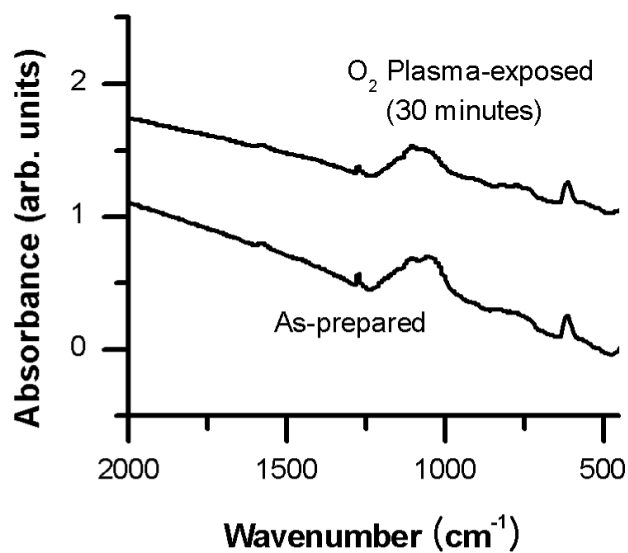
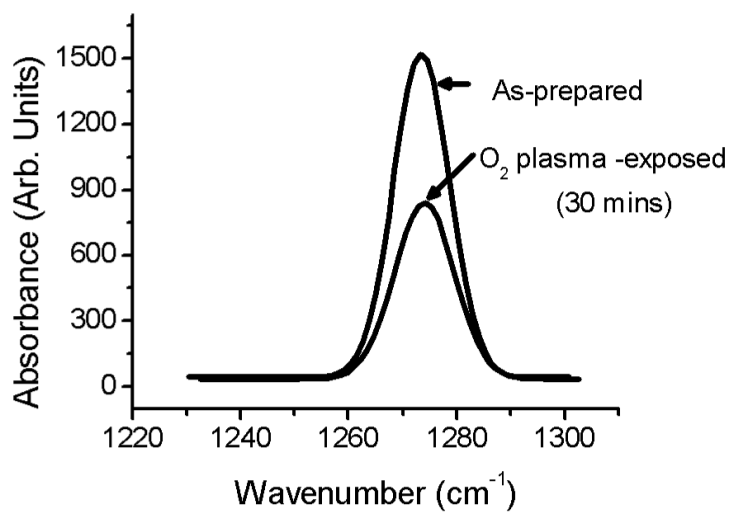


**Fig. 10.** Contact angle of (a) as-prepared film ( $126.8^\circ$ ) and after exposure to  $O_2$  plasma for (b) 15 seconds, (c) 30seconds and (d) 95 seconds ( $5.29^\circ$ ).

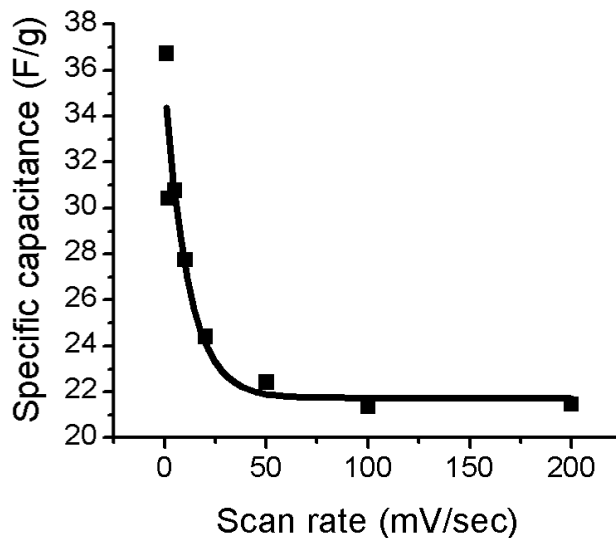


a

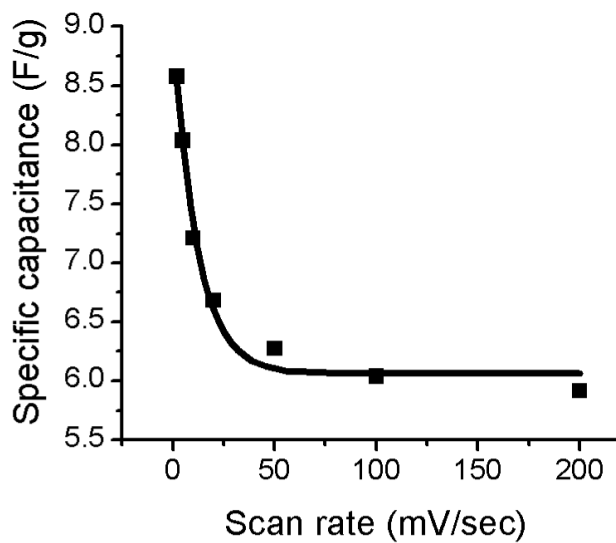


b

**Fig. 11.** FTIR spectra of as-prepared and O<sub>2</sub> plasma exposed sol-gel graphite thin film electrodes. (a) entire spectra. (b) spectra between 1280-1250 cm<sup>-1</sup> which corresponds to Si(CH<sub>3</sub>)<sub>n</sub>. There is 42.1% decrease in Si(CH<sub>3</sub>)<sub>n</sub> following oxygen plasma exposure.



a



b

**Fig. 12.** Plots of scan rate versus specific capacitance (F/g) of an aqueous solution containing 1 M KCl. The increase in capacitance at slow scan rates indicates the presence of micropores in the graphite/sol-gel films. (a) as-prepared electrode and (b) O<sub>2</sub> plasma treated electrode. The red curves show exponential fits of the data by the function:  $Ae^{-\tau/R} + B$ . For the as-prepared film  $A = 13.8$  F/g,  $B = 21.7$  F/g and  $R = 11.5$  mV/s. For the plasma-exposed film  $A = 2.95$  F/g,  $B = 6.06$  F/g and  $R = 11.9$  mV/s.